SINTEF
PROCEEDINGS
2

Proceedings of the 12th International Conference on Computational Fluid Dynamics in the Oil & Gas, Metallurgical and Process Industries

Progress in Applied CFD – CFD2017

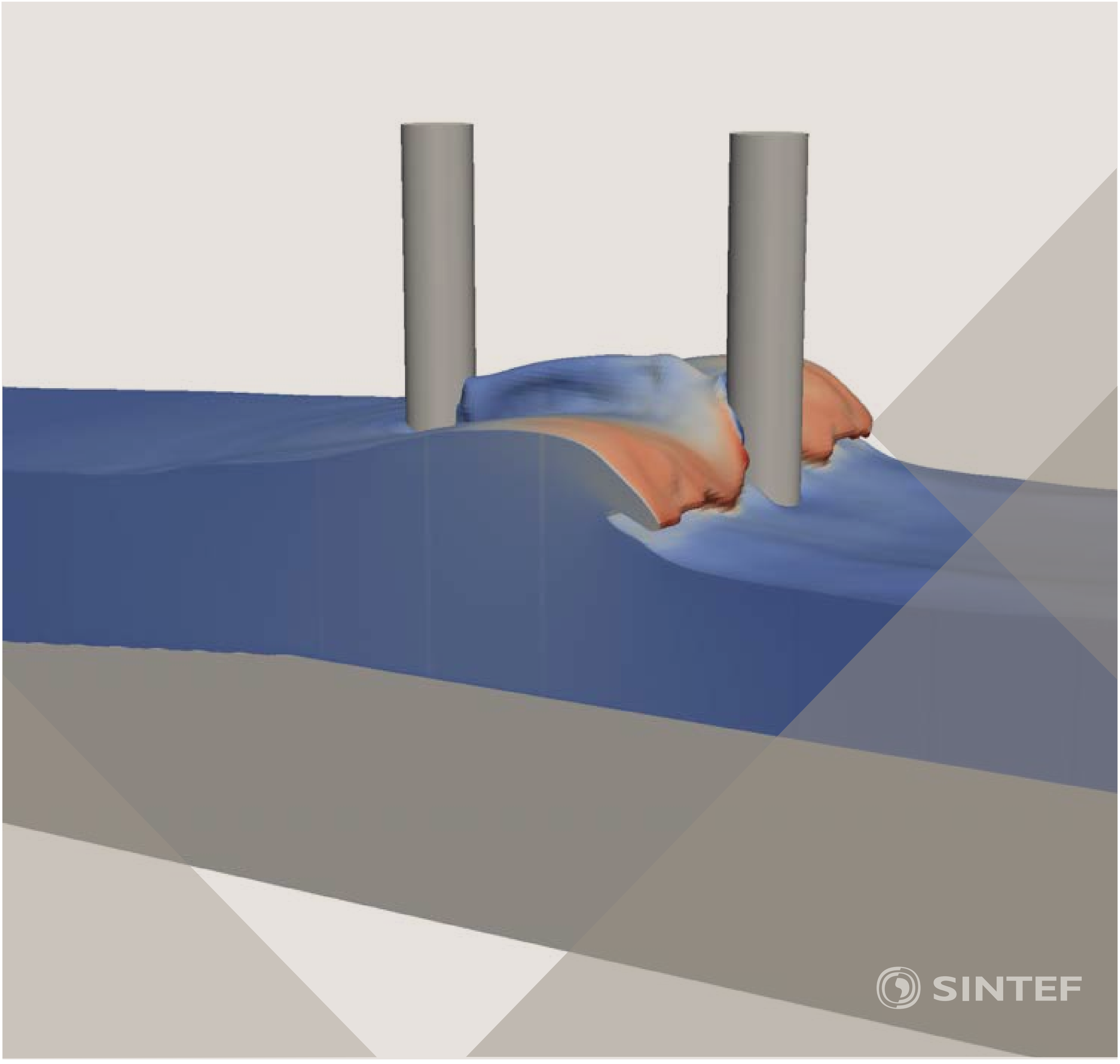

SINTEF Proceedings

Editors:
Jan Erik Olsen and Stein Tore Johansen

Progress in Applied CFD – CFD2017

Proceedings of the 12th International Conference on Computational Fluid Dynamics in the Oil & Gas, Metallurgical and Process Industries

SINTEF Academic Press

SINTEF Proceedings no 2
Editors: Jan Erik Olsen and Stein Tore Johansen
Progress in Applied CFD – CFD2017
Selected papers from 10th International Conference on Computational Fluid Dynamics in the Oil & Gas, Metallurgical and Process Industries

Key words:
CFD, Flow, Modelling

Cover, illustration: Arun Kamath

ISSN 2387-4295 (online)
ISBN 978-82-536-1544-8 (pdf)

SINTEF Academic Press

Address:	Forskningsveien 3 B
	PO Box 124 Blindern
	N-0314 OSLO
Tel:	+47 73 59 30 00
Fax:	+47 22 96 55 08

www.sintef.no/byggforsk
www.sintefbok.no

SINTEF Proceedings
SINTEF Proceedings is a serial publication for peer-reviewed conference proceedings on a variety of scientific topics.
The processes of peer-reviewing of papers published in SINTEF Proceedings are administered by the conference organizers and proceedings editors. Detailed procedures will vary according to custom and practice in each scientific community.

PREFACE

This book contains all manuscripts approved by the reviewers and the organizing committee of the 12th International Conference on Computational Fluid Dynamics in the Oil & Gas, Metallurgical and Process Industries. The conference was hosted by SINTEF in Trondheim in May/June 2017 and is also known as CFD2017 for short. The conference series was initiated by CSIRO and Phil Schwarz in 1997. So far the conference has been alternating between CSIRO in Melbourne and SINTEF in Trondheim. The conferences focuses on the application of CFD in the oil and gas industries, metal production, mineral processing, power generation, chemicals and other process industries. In addition pragmatic modelling concepts and bio-mechanical applications have become an important part of the conference. The papers in this book demonstrate the current progress in applied CFD.

The conference papers undergo a review process involving two experts. Only papers accepted by the reviewers are included in the proceedings. 108 contributions were presented at the conference together with six keynote presentations. A majority of these contributions are presented by their manuscript in this collection (a few were granted to present without an accompanying manuscript).

The organizing committee would like to thank everyone who has helped with review of manuscripts, all those who helped to promote the conference and all authors who have submitted scientific contributions. We are also grateful for the support from the conference sponsors: ANSYS, SFI Metal Production and NanoSim.

Stein Tore Johansen & Jan Erik Olsen

Organizing committee:

Conference chairman: Prof. Stein Tore Johansen
Conference coordinator: Dr. Jan Erik Olsen
Dr. Bernhard Müller
Dr.Sigrid Karstad Dahl
Dr.Shahriar Amini
Dr.Ernst Meese
Dr.Josip Zoric
Dr.Jannike Solsvik
Dr.Peter Witt

Scientific committee:

Stein Tore Johansen, SINTEF/NTNU
Bernhard Müller, NTNU
Phil Schwarz, CSIRO
Akio Tomiyama, Kobe University
Hans Kuipers, Eindhoven University of Technology
Jinghai Li, Chinese Academy of Science
Markus Braun, Ansys
Simon Lo, CD-adapco
Patrick Segers, Universiteit Gent
Jiyuan Tu, RMIT
Jos Derksen, University of Aberdeen
Dmitry Eskin, Schlumberger-Doll Research
Pär Jönsson, KTH
Stefan Pirker, Johannes Kepler University
Josip Zoric, SINTEF

CONTENTS

TOWARDS A CFD MODEL FOR BOILING FLOWS: VALIDATION OF QMOM PREDICTIONS WITH TOPFLOW EXPERIMENTS

Antonio BUFFO[1], **Marco VANNI**[1], **Daniele L. MARCHISIO**[1], **Gustavo MONTOYA**[2], **Emilio BAGLIETTO**[2]

[1]Department of Applied Science and Technology, Politecnico di Torino, ITALY

[2]Nuclear Science & Engineering, Massachussets Institute of Technology, USA

ABSTRACT

Boiling flows are very complex systems, usually confined in vertical pipes, where the liquid water moving upwards and the steam gas bubbles generated at the walls. The fluid dynamics of such systems is determined by the interplay of many different phenomena, including bubble nucleation, growth, condensation, coalescence, and breakage. For this reason, the development of a fully predictive computational fluid dynamics (CFD) model is very challenging, therefore we focus here only on some of the phenomena mentioned above (i.e. coalescence and breakage) by using population balance models (PBM). In this work, a coupled CFD-PBM model based on the two-fluid model and the quadrature method of moments (QMOM) was implemented in the open-source CFD code openFOAM. Simulation predictions obtained with this methodology are compared against the so-called TOPFLOW experiments for the first time, where simpler air-water cold systems that mimic the complexity of real boiling flows were investigated. Comparison between the available experimental data and the results show that great care must be paid on some modeling details, such as the inlet bubble size distribution (BSD) at the sparger and the coalescence and breakage rates modeling.

Keywords: Computational Fluid Dynamics, Population Balance Model, gas-liquid flows, top-flow experiments, boiling flow, coalescence, breakage, lift force. .

NOMENCLATURE

Greek Symbols

α Volume fraction, $[-]$.
β Daughter distribution function, $[1/m]$.
$\dot{\gamma}$ Shear strain rate, $[1/s^2]$.
δ Dirac delta function, $[-]$.
ε Turbulent dissipation rate, $[m^2/s^3]$.
κ Turbulent kinetic energy, $[m^2/s^2]$.
λ Collision efficiency, $[-]$.
μ Dynamic viscosity, $[kg/ms]$.
ρ Mass density, $[kg/m^3]$.
σ Surface tension, $[kg/s^2]$.
σ_κ $\kappa-\varepsilon$ model constant, $[-]$.
σ_ε $\kappa-\varepsilon$ model constant, $[-]$.
σ_{TD} Turbulent dispersion force parameter, $[-]$.
$\boldsymbol{\tau}$ Stress tensor, $[kg/ms^2]$.

Latin Symbols

a Coalescence kernel, $[m^3/s]$.
$\overline{b}_k$ Generic order moment of the daugther distribution function, $[m^k]$.
C Model constant or coefficient, $[-]$.
C_μ $\kappa-\varepsilon$ model constant, $[-]$.
$C_{\varepsilon,1}$ $\kappa-\varepsilon$ model constant, $[-]$.
$C_{\varepsilon,2}$ $\kappa-\varepsilon$ model constant, $[-]$.
d Diameter, $[m]$.
Eo Eötvös number, $[-]$.
$\mathbf{F}$ Interfacial force per unit volume, $[N/m^3]$.
G Turbulence production rate, $[m^2/s^3]$.
g Breakage frequency, $[1/s]$.
$\mathbf{g}$ Gravity, $[m/s^2]$.
h Collision frequency, $[m^3/s]$.
$\mathbf{I}$ Identity matrix, $[-]$.
L Quadrature node (bubble size), $[m]$.
M_k k-th order moment, $[m^{k-3}]$.
n Number density function, $[1/m^4]$.
p Pressure, $[Pa]$.
Re Reynolds number, $[-]$.
$\mathbf{S}$ Strain rate tensor, $[1/s]$.
$\overline{S}_k$ Generic order moment transport equation source term, $[m^{k-3}/s]$.
t Time, $[s]$.
$\mathbf{U}$ Velocity, $[m/s]$.
w Quadrature weight, $[1/m^3]$.
We Weber number, $[-]$.

Sub/superscripts

α Index α.
b Bubbly gas phase.
$buoy$ Buoyancy.
D Drag.
$eddy$ Eddy.
eff Effective.
i Index i.
j Index j.
k Index k.
l Liquid phase.
L Lift or bubble size.
$shear$ Macroscopic shear.
t Turbulent.
T Terminal.
TD Turbulent dispersion.
tf Turbulent fluctuations.
VM Virtual Mass.
$wake$ Wake.

Abbreviations
BSD Bubble Size Distribution.
CFD Computational Fluid Dynamics.
CFL Courant-Friedrichs-Lewy.
MOC Methods of Classes.
NDF Number Density Function.
PBE Population Balance Equation.
PBM Population Balance Model.
QBMM Quadrature-Based Moment Method.
QMOM Quadrature Method Of Moments.

INTRODUCTION

Boiling flows are omnipresent in the chemical, process and nuclear industries. Generally, the flow is confined in vertical pipes, with liquid water moving upwards and steam gas bubbles formed (via nucleation) at the wall and undergoing subsequent coalescence, breakage, growth and condensation. The movement of the steam gas bubbles is dictated by the interfacial forces, notably drag, lift and turbulent dispersion. In this particular flow configuration, the lift force plays a crucial role, as it is the main force pushing the bubbles away from the wall and into the core of the flow. The simulation of such flows is a challenge because of the variety and complexity of the phenomena involved, particularly the nucleation of gas bubbles at the wall and the interplay between interfacial forces, coalescence and breakage. In order to simplify the problem focusing only on fluid dynamics, very often steam bubble's nucleation, growth and condensation are not considered and the process investigated consists mainly on the injection of air bubbles at the wall, into a flow of cold water, mimicking the actual boiling flow (Schaffrath *et al.*, 2001; Prasser *et al.*, 2005; Lucas *et al.*, 2007). Computational fluid dynamics (CFD) coupled with population balance models (PBM) is commonly used to simulate such flows, by means of the Eulerian-Eulerian two-fluid model for the description of the air-water flow and the method of classes (MOC) for the solution of the PBM for the gas bubbles. However, this method is quite expensive and alternatives have been recently explored. In this work we want to replace the MOC with quadrature-based moments methods (QBMM) for the solution of the PBM. Among the different possible choices, QMOM is considered and different couplings with the CFD model are studied. In particular, the effect of the inlet bubble diameter on the final results is investigated. Moreover, different correlations for the interfacial forces (i.e. drag, lift, virtual mass and turbulent dispersion force), as well as different kernels for coalescence and breakage are here reviewed and analyzed, with the aim to be investigated in future communications. Simulations are performed with the open-source CFD code openFOAM by using the solver `compressibleTwoPhaseEulerFoam`, implementing the two-fluid model. The solver has been extensively modified to include QMOM, as illustrated in our previous work (Buffo *et al.*, 2016b). Simulation predictions are validated against the so-called TOPFLOW experiments (Prasser *et al.*, 2005; Lucas *et al.*, 2010), by comparing the bubble size distribution (BSD), the radial profiles of gas and liquid velocities, as well as gas volume fraction, at different heights of the test rig and under different operating conditions.

MODEL DESCRIPTION

As previously mentioned, the Eulerian-Eulerian two-fluid model is here adopted to predict the behavior of the boiling flow. The governing equations are briefly presented in the following (Buffo and Marchisio, 2014):

$$\frac{\partial \rho_k \alpha_k}{\partial t} + \nabla \cdot (\rho_k \alpha_k \mathbf{U}_k) = 0, \tag{1}$$

$$\frac{\partial \rho_k \alpha_k \mathbf{U}_k}{\partial t} + \nabla \cdot (\rho_k \alpha_k \mathbf{U}_k \mathbf{U}_k) = - \nabla \cdot (\alpha_k \boldsymbol{\tau}_k) - \alpha_k \nabla p + \alpha_k \rho_k \mathbf{g} + \mathbf{F}_k, \tag{2}$$

where the subscript k is equal to l for the continuous liquid phase and b for the bubbly gaseous phase, and where α_k is the volume fraction, ρ_k is the density and $\mathbf{U}_k$ is the Reynolds-averaged velocity for phase k. For instance, the stress tensor of the liquid phase $\boldsymbol{\tau}_l$ is modeled considering a Newtonian fluid and the Boussinesq approach:

$$\boldsymbol{\tau}_l = \mu_{\mathrm{eff,l}} \left((\nabla \mathbf{U}_l) + (\nabla \mathbf{U}_l)^T - \frac{2}{3} \mathbf{I} (\nabla \cdot \mathbf{U}_l) \right) \tag{3}$$

where $\mu_{\mathrm{eff,l}}$ is the effective viscosity of the liquid phase: $\mu_{\mathrm{eff,l}} = \mu_l + \mu_{t,l}$, and where in turn μ_l is the molecular viscosity of the liquid and $\mu_{t,l} = \rho_l C_\mu \frac{\kappa^2}{\varepsilon}$, κ is the turbulent kinetic energy of the liquid phase and ε is the energy dissipation rate of the liquid phase. These two quantities are here calculated by using the multiphase extension of the $\kappa - \varepsilon$ model (Kataoka and Serizawa, 1989), since it represents a good compromise between accuracy and computational time:

$$\frac{\partial \alpha_l \kappa}{\partial t} + \nabla \cdot (\alpha_l \kappa \mathbf{U}_l) - \nabla \cdot \left(\alpha_l \frac{\mu_{t,l}}{\rho_l \sigma_\kappa} \nabla \kappa \right) = \alpha_l (G - \varepsilon), \tag{4}$$

$$\frac{\partial \alpha_l \varepsilon}{\partial t} + \nabla \cdot (\alpha_l \varepsilon \mathbf{U}_l) - \nabla \cdot \left(\alpha_l \frac{\mu_{t,l}}{\rho_l \sigma_\varepsilon} \nabla \varepsilon \right) = \alpha_l \left(C_{\varepsilon,1} \frac{\varepsilon}{\kappa} G - C_{\varepsilon,2} \frac{\varepsilon^2}{\kappa} \right). \tag{5}$$

The model constants are those of the standard $\kappa - \varepsilon$ model: $C_\mu = 0.09$, $\sigma_\kappa = 1.0$, $\sigma_\varepsilon = 1.3$, $C_{\varepsilon,1} = 1.44$, and $C_{\varepsilon,2} = 1.92$. The term G is the turbulence production rate defined as: $G = 2 \frac{\mu_{t,l}}{\rho_l} (\mathbf{S} : \nabla \mathbf{U}_l)$, where the strain rate tensor is in turn defined as $\mathbf{S} = \frac{1}{2} \left(\nabla \mathbf{U}_l + (\nabla \mathbf{U}_l)^T \right)$.
It is important to remark that the term $\mathbf{F}_k$ in Eq. (2) is crucial for a proper description of the fluid dynamics, since it is responsible for the momentum coupling between the phases by considering the different interfacial forces. Such term is usually described as a summation of different contributions, such as drag, lift, virtual mass, turbulent dispersion and wall lubrication forces (Lucas *et al.*, 2007; Buffo and Marchisio, 2014; Sugrue *et al.*, 2017). Although for standard equipment configurations as stirred tanks and bubble columns most of them can be neglected apart from the drag force (Buffo *et al.*, 2016a), in small diameter vertical pipes typical of boiling flows, where also the liquid phase raises through the column, and the gas is injected or formed laterally and then migrating towards the center of the column, all the forces may play a role (Lucas *et al.*, 2007; Lucas and Tomiyama, 2011). Therefore the term $\mathbf{F}_b$ can be written as:

$$\mathbf{F}_b = -\mathbf{F}_l = \mathbf{F}_D + \mathbf{F}_L + \mathbf{F}_{VM} + \mathbf{F}_{TD}. \tag{6}$$

The drag force per unit volume F_D can be expressed as:

$$\mathbf{F}_D = -\frac{3}{4} \frac{\alpha_b \rho_l C_D}{d_b} |\mathbf{U}_b - \mathbf{U}_l| (\mathbf{U}_b - \mathbf{U}_l), \tag{7}$$

where d_b is the bubble diameter and C_D is the drag coefficient, which is here evaluated using the Tomiyama drag law (for slightly contaminated liquid) (Tomiyama *et al.*, 1998):

$$C_D = \max\left(\min\left(\frac{24}{\mathrm{Re}_b}\left(1+0.15\mathrm{Re}_b^{0.687}\right), \frac{72}{\mathrm{Re}_b}\right), \frac{8}{3}\frac{\mathrm{Eo}}{\mathrm{Eo}+4}\right) \tag{8}$$

where the bubble Reynolds number Re_b and the Eötvös number Eo can be written as:

$$\mathrm{Re}_b = \frac{\rho_l|\mathbf{U}_b - \mathbf{U}_l d_b}{\mu_l}, \tag{9}$$

$$\mathrm{Eo} = \frac{g(\rho_l - \rho_b)d_b^2}{\sigma} \tag{10}$$

where σ is the surface tension and g is the gravity acceleration. The lift force per unit volume F_L can be written as (Lucas *et al.*, 2007):

$$\mathbf{F}_L = -C_L\alpha_b\rho_l(\mathbf{U}_b - \mathbf{U}_l)\times(\nabla\times\mathbf{U}_l), \tag{11}$$

where C_L is the lift coefficient. As can be observed in Eq. (6), in this work we do not model the wall lubrication as a separate force. We used the model of Shaver and Podowski (2015), where the wall lubrication phenomena is described by adjusting the lift coefficient according to the distance from the wall:

$$\begin{cases} 0 & \text{if } \frac{y}{d_b} < \frac{1}{2} \\ C_{L,0}\left(3\left(2\frac{y}{d_b}-1\right)^2 - 2\left(2\frac{y}{d_b}-1\right)^3\right) & \text{if } \frac{1}{2} \le \frac{y}{d_b} \le 1 \\ C_{L,0} & \text{if } 1 < \frac{y}{d_b} \end{cases} \tag{12}$$

The virtual mass force force can be expressed as (Lucas *et al.*, 2007):

$$\mathbf{F}_{VM} = -\alpha_b\rho_l C_{VM}\left(\frac{D\mathbf{U}_b}{Dt} - \frac{D\mathbf{U}_l}{Dt}\right), \tag{13}$$

where C_{VM} is the virtual mass coefficient and $\frac{D}{Dt}$ is the substantial derivative. The turbulent dispersion force per unit volume F_{TD} can be written as (Burns *et al.*, 2004):

$$\mathbf{F}_{TD} = -\frac{3}{4}\frac{C_D\alpha_b\mu_{l,t}}{d_b\sigma_{TD}}|\mathbf{U}_b - \mathbf{U}_l|\left(\frac{1}{\alpha_l}+\frac{1}{\alpha_b}\right)\nabla\alpha_b, \tag{14}$$

where σ_{TD} is a constant equal to unity.

This short overview about the different interfacial forces is here reported for the sake of completeness. It is worth remarking here that, in this work, we focused on the population balance modeling (PBM). As far as the interfacial forces are concerned, we started including into the model gravity, buoyancy and drag, leaving the analysis of the effect of the different interfacial forces for future communications.

It is worth also remarking that in this investigation bubble nucleation and condensation are neglected, even though both are essential features of the boiling flows. In fact, the test cases simulated is a air-water system, where air bubbles are injected laterally to mimics the fluid dynamics of boiling flows. Bubble nucleation and condensation do not occur in this case and therefore they are neglected.

It is also useful to mention that the bubble diameter d_b appearing in Eq. (7) refers to the idealized monodisperse bubble distribution introduced with the two-fluid model. When a polydisperse bubble distribution is considered as in this case, d_b refers to the so-called mean Sauter diameter (d_{32}) which is the ratio between the moment of order three and the moment of order two with respect to the bubble size. We will see in the following how to calculate this last term through the PBM.

Population balance modeling

The PBM is based on the solution of the Population Balance Equation (PBE). For a thorough discussion on this equation, the reader may refer to the specialized literature (Ramkrishna, 2000; Marchisio and Fox, 2013). Among many methods to solve such complex integro-differential equation, the method here used is the Quadrature Method of Moments (QMOM) (Marchisio and Fox, 2013), which is based on the idea to approximate the bubble size distribution (BSD), $n(L)$, as a summation of Dirac delta functions :

$$n(L) \approx \sum_{\alpha=1}^{N} w_\alpha\delta(L - L_\alpha), \tag{15}$$

where w_α and L_α are the N weights and nodes of the quadrature approximation of order N and L is the bubble size. The nodes and weights can be calculated from the first $2N$ moments of the BSD, with the generic order moment M_k being defined as:

$$M_k = \int_0^\infty n(L)L^k \mathrm{d}L \approx \sum_{\alpha=1}^{N} w_\alpha L_\alpha^k, \tag{16}$$

where $k \in 0,\ldots,2N-1$ is the moment order. The way in which the weights and nodes of quadrature can be calculated from the moments is by means of the so-called moment inversion algorithms, such as for example the Product-Difference and Wheeler algorithms (Marchisio and Fox, 2013). The evolution of the generic order moment in space and time can be evaluated through the solution of the following transport equation:

$$\frac{\partial M_k}{\partial t} + \nabla\cdot(\mathbf{U}_b M_k) = \overline{S}_k, \tag{17}$$

which is derived from the PBE by applying the moment transform to such equation. In this way, the closure problem is solved, since the source term of Eq. (17) can be written as a function of the quadrature weights and nodes:

$$\overline{S}_k \approx \frac{1}{2}\sum_{\alpha=1}^{N}\sum_{\beta=1}^{N} w_\alpha w_\beta a_{\alpha,\beta}\left[\left(L_\alpha^3 + L_\beta^3\right)^{k/3} - L_\alpha^k - L_\beta^k\right] + \sum_{\alpha=1}^{N} w_\alpha g_\alpha\left(\overline{b}_\alpha^k - L_\alpha^k\right), \tag{18}$$

where $a_{\alpha,\beta} = a(L_\alpha, L_\beta)$ is the coalescence kernel, $g_\alpha = g(L_\alpha)$ is the breakage kernel and:

$$\overline{b}_\alpha^k = \int_0^\infty L^k\beta(L|L_\alpha)\,\mathrm{d}L. \tag{19}$$

is the generic order moment of the daughter distribution function $\beta(L|L_\alpha)$. The value of the diameter d_b to be used in the expressions of the previous section can be calculated from the moments of the BSD. For instance the mean Sauter diameter is defined as follows:

$$d_b = d_{32} = \frac{M_3}{M_2}. \tag{20}$$

These models are essential for the proper solution of the PBM, since they represent the link between the mathematical method and the investigated physical phenomena. In this work, we expressed the coalescence kernel in the following way:

$$a(L',L) = h(L',L)\lambda(L',L), \tag{21}$$

where $h(L',L)$ is the collision frequency and $\lambda(L',L)$ is the coalescence efficiency. The first term can be estimated by considering all the physical mechanisms that bring two bubbles close to each other and collide, while the second term relates the contact time during the collision and the time needed for the liquid film drainage between the colliding bubbles. The collision frequency is expressed as follows (Liao and Lucas, 2010; Liao *et al.*, 2015):

$$h(L',L) = h_{tf} + h_{shear} + h_{eddy} + h_{buoy} + h_{wake}, \tag{22}$$

where the first term accounts for the collisions induced by the turbulent fluctuations, the second for those by the macroscopic shear, the third for those due to bubbles trapped into large eddies, the forth due to different terminal velocities given by the act of body forces (such as buoyancy) and the last term due to the small bubbles entrainment into the wake of large bubbles. It is important to remark that with Eq. (22) it is assumed that there are no interactions between these different mechanisms, in such a way that the frequencies can be summed up to give the overall coalescence frequency. This approximation is totally arbitrary from a physical point of view, although it is very complex to quantify the interactions between the different coalescence mechanisms.

For h_{tf} we used the well known model of Coulaloglou and Tavlarides (1977):

$$h(L',L)_{tf} = C_{tf}\frac{\pi}{4}(L'+L)^2(L'^{2/3}+L^{2/3})^{1/2}\varepsilon^{1/3}. \tag{23}$$

where C_{tf} is a model constant, equal to 0.88 from the theory but can be adjusted to fit different systems. For h_{shear} the model reported in the work of Liao *et al.* (2015) is used:

$$h(L',L)_{shear} = C_{shear}\frac{1}{8}(L'+L)^3\dot{\gamma}_c, \tag{24}$$

where C_{shear} is parameter of the model and $\dot{\gamma}_c$ is the shear strain rate of the continuous phase flow. A similar expression has also the term h_{eddy} (Liao *et al.*, 2015):

$$h(L',L)_{eddy} = C_{eddy}\frac{1}{8}(L'+L)^3\dot{\gamma}_{eddy}, \tag{25}$$

where C_{eddy} is parameter of the model and the eddy shear strain rate $\dot{\gamma}_{eddy}$ can be written as follows:

$$\dot{\gamma}_{eddy} = \sqrt{\frac{\rho_l\varepsilon}{\mu_l}}. \tag{26}$$

The coalescence frequency due to body forces interactions, $h(L',L)_{buoy}$, can be estimated by considering the terminal velocities of the interacting bubbles as follows (Liao *et al.*, 2015):

$$h(L',L)_{buoy} = C_{buoy}\frac{\pi}{4}(L'+L)^2|U_{T,L'}-U_{T,L}|, \tag{27}$$

where C_{buoy} is a constant parameter and $U_{T,L}$ is the terminal velocity of the bubble with size L and can be assessed by means of well known correlations. The last term of Eq. (22) accounting for the bubble wake-entrainment is here calculated by using the model of Wang *et al.* (2005):

$$h(L',L)_{wake} = C_{wake}\frac{\pi}{4}\left[L'^2U_{T,L'}C_{D,L'}^{1/3}\Theta_{L'} + L^2U_{T,L}C_{D,L}^{1/3}\Theta_L\right], \tag{28}$$

where C_{wake} is a model constant, $C_{D,L}$ is the drag coefficient for the bubble with size L, while Θ_L is a function with the following expression (Wang *et al.*, 2005):

$$\Theta = \begin{cases} \dfrac{(L'-\frac{1}{2}L_{crit})^6}{(L'-\frac{1}{2}L_{crit})^6+(\frac{1}{2}L_{crit})^6} & \text{se } L' \geq \frac{1}{2}L_{crit}; \\ 0 & \text{otherwise.} \end{cases} \tag{29}$$

The critical diameter L_{crit} can be assumed equal to 10 mm in air-water systems, or can be estimated through the following equation:

$$L_{crit} = 4.0\sqrt{\frac{\sigma}{g(\rho_c-\rho_d)}}. \tag{30}$$

In this work, we restricted our analysis only on coalescence caused by turbulent fluctuations. Other coalescing mechanisms will be taken into account in future works.

The last missing portion of physics to estimate the coalescence kernel written in Eq. (21) is the coalescence efficiency $\lambda(L',L)$. With this simplified approach, a unique coalescence efficiency multiplies the overall coalescence frequency, although in principle each coalescence mechanism has its own efficiency. In the work of Liao *et al.* (2015), indeed the overall coalescence efficiency is calculated in such a way to consider all the coalescing mechanisms of Eq. (22), but it is assumed that the less efficient collision is the limiting efficiency, which might be a too strong approximation of the physical phenomena. For this reason, in this work we started by considering only the efficiency due to turbulent fluctuations λ_{tf}, and then all the other mechanisms will be progressively taken into account in the future. Different models were here considered, as the standard model of Coulaloglou and Tavlarides (1977), which is based on ratio between drainage and contact time:

$$h_{ft}(L',L) = \exp\left\{-C_{tf}\frac{\mu_l\rho_l\varepsilon}{\sigma^2}\left(\frac{L'L}{L'+L}\right)^4\right\} \tag{31}$$

with the dimensioned parameter C_{tf} (m^{-2}) being fitted with experimental data. In this work, the standard value of $6\cdot10^9$ m^{-2} is used. Another possible approach is the one given by Chesters (1991), which depends on bubbles Weber number, namely on the ratio between kinetic energy of the collision and the resisting surface energy to coalescence:

$$h_{ft}(L',L) = \exp\left\{-C_{We}\sqrt{We_{i,j}}\right\} \tag{32}$$

where $We_{i,j}$ is the Weber number defined as follows:

$$We_{i,j} = \frac{\rho_l\varepsilon^{2/3}}{\sigma}\frac{L_iL_j}{L_i+L_j}(L_i^{2/3}+L_j^{2/3}). \tag{33}$$

Regarding the breakage kernel, the model of Laakkonen *et al.* (2007) based on the homogeneous isotropic turbulence theory and considering the size of the mother bubble compatible with the eddy length scale of the inertial subrange is here adopted:

$$g(L) = C_1\varepsilon^{1/3}\mathrm{erfc}\left(\sqrt{C_2\frac{\sigma}{\rho_l\varepsilon^{2/3}L^{5/3}} + C_3\frac{\mu_l}{\sqrt{\rho_l\rho_b}\varepsilon^{1/3}L^{4/3}}}\right) \tag{34}$$

where $C_1 = 6.0$, $C_2 = 0.04$ and $C_3 = 0.01$ as in our previous works on gas-liquid systems (Buffo and Marchisio, 2014; Buffo *et al.*, 2016a). Although this is not the only breakage mechanism occurring in a real system, it is indeed the most important and therefore the first to be considered here as a first approximation (Laakkonen *et al.*, 2006, 2007). Indeed, this aspect will be further investigated in future communications.

As far as the daughter distribution function is concerned, the following β−distribution function is used (Laakkonen *et al.*, 2006):

$$\beta(L,L') = 180\left(\frac{L^2}{L'^3}\right)\left(\frac{L^3}{L'^3}\right)^2\left(1-\frac{L^3}{L'^3}\right)^2 \qquad (35)$$

where L is the size of the daughter bubble, created by the breakage of the mother bubble of size L'. This distribution is a bell-shaped distribution, where the symmetric breakage is the most probable event, due to the "activated" state in which the mother bubble is equilibrated by surface tension into two equally-sized fragments just before breaking. This choice was supported by comparison with experiments in previous works (Laakkonen *et al.*, 2006, 2007; Buffo *et al.*, 2016a). However other opposite approaches are debated in the literature, such as U-shaped and M-shaped distributions. The reader may refer to Liao and Lucas (2009) for further discussion.

TEST CASE AND NUMERICAL DETAILS

As previously mentioned, the experimental setup here investigated for validation purposes is the TOPFLOW rig built at Helmholtz-Zentrum Dresden-Rossendorf (HZDR) (Schaffrath *et al.*, 2001; Prasser *et al.*, 2005; Lucas *et al.*, 2010). This system consist of a vertical pipe of 195.3 mm diameter and 8000 mm tall, where liquid water raises from the bottom to the top of the column and air is injected laterally from holes placed at fixed distance along the circumference and at different heights of the column. The measurement apparatus is instead located at a fixed height of the vertical pipe, and it is composed by a mesh-wire sensor able to locally measure some of the most important property of the gas-liquid flow, such as the radial profiles of void fraction, gas velocity and bubble size distribution. Over the years a significant number of operating conditions were investigated by varying both liquid and gas flow rates, as exemplified in Table 1, where a small subset of the experiments carried out is reported.

Table 1: Some of the operating conditions investigated. Each number corresponds to a particular operating condition.

		Superf. gas vel. (m/s)				
		0.0025	**0.004**	**0.0062**	**0.0096**	**0.0235**
Superf. liq. vel. (m/s)	**2.554**	010	021	032	043	065
	1.611	009	020	031	042	064
	1.017	008	019	030	041	063
	0.405	006	017	028	039	061
	0.102	003	014	025	036	058

Our own implementation of QMOM into the OpenFOAM (version 2.2.x) solver `compressibleTwoPhaseEulerFoam` was used to perform the three-dimensional transient numerical simulations. This implementation includes the transport equation for the moments of the BSD, and the Wheeler inversion algorithm to calculate the quadrature approximation from the transported moments (Buffo *et al.*, 2016b) and the calculation of the different submodels for the interfacial forces and the coalescence and breakage rates. In this work, only the first six moments of the BSD were calculated (M_0, M_1, M_2, M_3, M_4, M_5), corresponding to a quadrature approximation with three nodes: $N = 3$. Particular attention was paid to the problem of moment boundedness and realizability by means of a proper implementation of the moment transport equations (Buffo *et al.*, 2016b). As far as the inlet boundary conditions for the BSD is concerned, we adopted the same condition as our previous works (Buffo *et al.*, 2013, 2016a,b, 2017): a lognormal bubble size distribution with a standard deviation equal to 15% of the mean value, as suggested by Laakkonen *et al.* (2006) for holed sparger, and a mean value estimated through correlations or experimental evidences.

Different modeling aspects were taken into account in this work. First, a sensitivity analysis has been performed on the value of the inlet mean bubble diameter in order to assess the influence of this parameter on the predictions obtained with the PBM. The obtained results were also compared to the ones given by using the relationship of Changjun *et al.* (2013) to estimate the mean inlet bubble diameter, which takes into account the effect of the hole orientation in the physical space on the inlet mean bubble size. This procedure of Changjun *et al.* (2013) is based on the solution of ordinary differential equations for the position of the center of mass of the formed bubble and it is based on the balance of forces acting on the bubble before detaching from the sparger, namely buoyancy, gravity, drag, lift and virtual mass. Further details on its implementation can be found in the original work (Changjun *et al.*, 2013). Among all the operating conditions available, we picked the 008 and 042 points from Table 1, with the first operating condition corresponding to a gas superficial velocity of 0.0025 m s^{-1} and a liquid superficial velocity of 1.017 m s^{-1} and the second 0.096 m s^{-1} and 1.611 m s^{-1} respectively. It is worth mentioning that in all the performed simulations only the gravity, buoyancy and drag forces were considered as a first approximation. An in-depth analysis on the importance of different interfacial forces, especially to simulate operating conditions with higher gas superficial velocities is left to future communications.

RESULTS

Let us start the discussion of the results with the sensitivity analysis on the inlet bubble size. This aspect is particularly important when a CFD-PBM approach is used, since different boundary conditions may lead to different solutions and there is always a certain degree of uncertainties about the estimations of the inlet bubble size through experiments or correlations. Fig. 1 shows the comparison between experimental data and numerical predictions for the axial profiles of the surface-averaged mean Sauter diameter for different values of the mean inlet bubble diameter. As it is possible to observe from the figure, all the simulations with the different inlet bubble diameter values shows a different initial part of the axial profile (i.e., close to the bubble injection section), while all reach approximately the same asymptotic value at the highest section of the vertical profile. This result is of great importance, since it proves that the steady-state reached by the system is not sensitive to this modeling parameter. Moreover, the profile obtained with the inlet value calculated with the correlation of Changjun *et al.* (2013) (i.e., 4.15 mm) is very close to the experimental points close to inlet section, while differs far from the inlet.

This mismatch can be caused by the approximations performed in the evaluation of the coalescence rates: at the moment in the model only the turbulent fluctuations are considered and most likely in the higher sections of the vertical pipe other mechanisms may become important, such as the body forces (buoyancy) or macroscopic shear rate mechanisms.

It is also interesting have a look at the radial profiles of volume fraction and axial gas velocity at different heights of the column. Figs. 2 and 3 report these two properties of the gas-liquid systems for the operating condition 008 (gas superficial velocity of 0.0025 m s^{-1} and liquid superficial velocity of 1.017 m s^{-1}), while Figs. 4 and 5 for the operating condition 042 (gas superficial velocity of 0.096 m s^{-1} and liquid superficial velocity of 1.611 m s^{-1}).

At it can be seen from the figures, the agreement with the experimental data is decent for both the analyzed properties and for both the operating conditions.

The largest deviation from the experimental data is observed for the closest and farthest sections from the inlet for both operating conditions for the local volume fraction profiles. It is worth reminding here that model at the moment does not consider any other additional interfacial forces apart from gravity, buoyancy and drag, as a first approximation. Therefore, the deviation observable is most likely due to this aspect: in fact, it is clear that close to the gas inlet the bubbles are

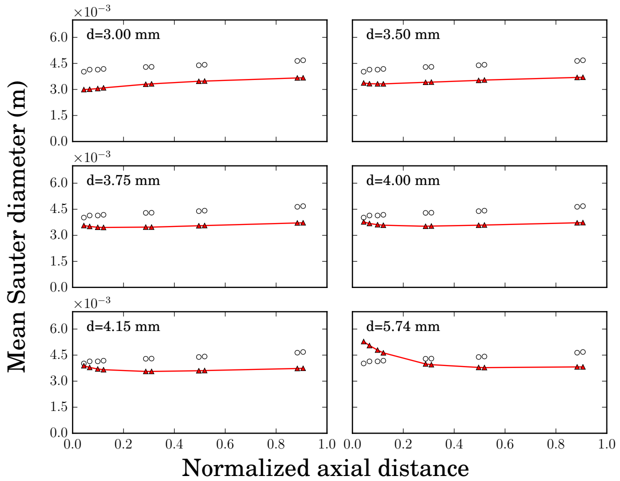

Figure 1: Axial profiles of the surface-averaged mean Sauter diameter for different values of the mean inlet bubble diameter. Operating condition 008. White circles: experimental data. Red triangles: simulation results

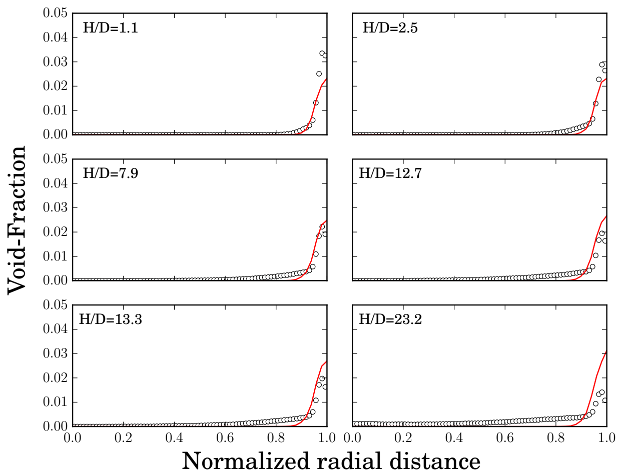

Figure 2: Void fraction radial profiles at different heights of the vertical pipe. Operating condition 008. White circles: experimental data. Red line: numerical results.

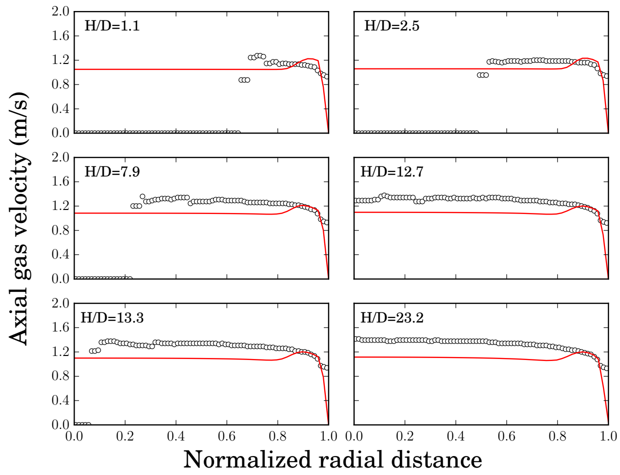

Figure 3: Axial velocity radial profiles at different heights of the vertical pipe. Operating condition 008. White circles: experimental data. Red line: numerical results.

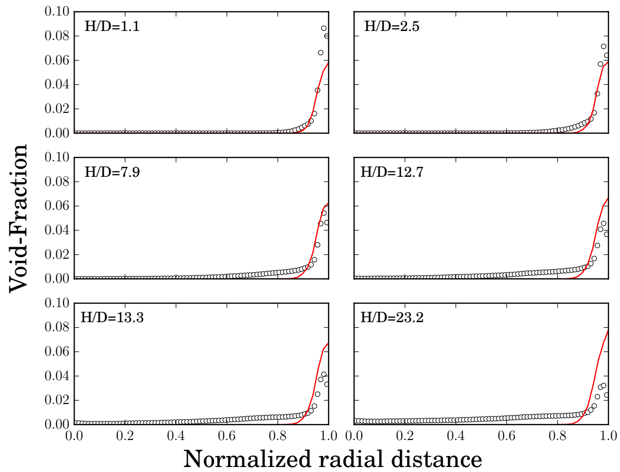

Figure 4: Void fraction radial profiles at different heights of the vertical pipe. Operating condition 042. White circles: experimental data. Red line: numerical results.

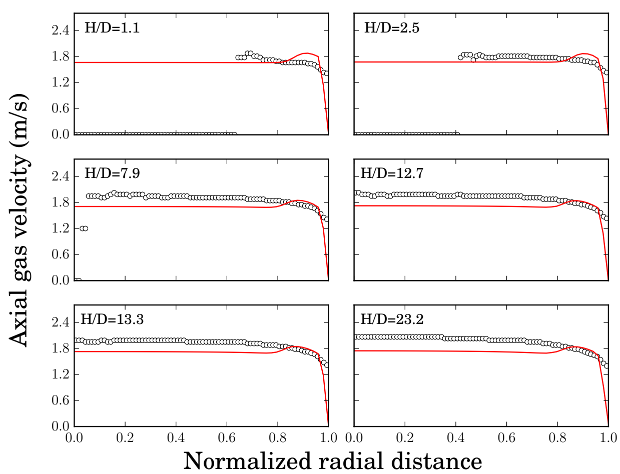

Figure 5: Axial velocity radial profiles at different heights of the vertical pipe. Operating condition 042. White circles: experimental data. Red line: numerical results.

small and the lift force tends to push them towards the wall, while for the highest values of the vertical pipe (where the bubbles are bigger due to coalescence) the turbulence dispersion force becomes important and moves the bubbles from the walls to the core of the vertical pipe.

From the comparison between the experimental data and the numerical predictions in terms of the axial gas velocity profiles reported in Figs. 3 and 5 it is instead possible to note that the agreement is good in the region close to the wall, where most of the bubbles can be found. When the normalized radial distance is lower than 0.9, the values of axial gas velocity do not have any physical meaning, since only few bubbles can be experimentally detected.

CONCLUSION

In this work, a CFD-PBM methodology was applied to the simulation of an air-water system that mimics the conditions of a boiling flow, notably the TOPFLOW experiments. Simulations were performed with the open-source CFD code OpenFOAM (version 2.2.x) by using a modified version of the solver `compressibleTwoPhaseEulerFoam` which contains our own implementation of QMOM.

A sensitivity analysis on the boundary conditions for the PBM shows that the steady-state solution is not influenced by the inlet bubble diameter; moreover, the value of such parameter given by the model of Changjun *et al.* (2013) is able to reproduce well the behavior of the BSD in the regions close to the inlet sections. The comparison between experiments and predictions in terms of the void fraction and axial gas velocity profiles for two operating conditions available shows a good agreement, however an in-depth analysis on the effect of the different interfacial forces and the different coalescence mechanisms is need for the development of a general modeling tool that can be used for a larger number of operating conditions experimentally investigated.

ACKNOWLEDGEMENTS

The authors wish to thank Prof. Dirk Lucas at Helmholtz-Zentrum Dresden-Rossendorf (HZDR). Access to the TOPFLOW data was kindly provided by HZDR in the framework of the HZDR-MIT collaboration. Moreover, the authors gratefully thank Salvatore Falzone, Mohsen Shia and Umberto Viscomi for their valuable contributions to this work. The financial support of the MITOR Project (Compagnia di San Paolo) is gratefully acknowledged.

REFERENCES

BUFFO, A., VANNI, M., RENZE, P. and MARCHISIO, D. (2016a). "Empirical drag closure for polydisperse gasâĂŞliquid systems in bubbly flow regime: Bubble swarm and micro-scale turbulence". *Chemical Engineering Research and Design*, **113**, 284–303.

BUFFO, A., VANNI, M. and MARCHISIO, D. (2016b). "On the implementation of moment transport equations in OpenFOAM: Boundedness and realizability". *International Journal of Multiphase Flow*, **85**, 223–235.

BUFFO, A., VANNI, M. and MARCHISIO, D. (2017). "Simulation of a reacting gasâĂŞliquid bubbly flow with CFD and PBM: Validation with experiments". *Applied Mathematical Modelling*, **44**, 43–60.

BUFFO, A. and MARCHISIO, D.L. (2014). "Modeling and simulation of turbulent polydisperse gas-liquid systems via the generalized population balance equation". *Reviews in Chemical Engineering*, **30(1)**, 73–126.

BUFFO, A., MARCHISIO, D.L., VANNI, M. and RENZE, P. (2013). "Simulation of polydisperse multiphase systems using population balances and example application to bubbly flows". *Chemical engineering research and design*, **91(10)**, 1859–1875.

BURNS, A.D., FRANK, T., HAMILL, I. and SHI, J.M. (2004). "The favre averaged drag model for turbulent dispersion in eulerian multi-phase flows". *5th international conference on multiphase flow, ICMF*, vol. 4, 1–17.

CHANGJUN, L., LIANG, B., SHENGWEI, T. and ENZE, M. (2013). "Effects of orifice orientation and gas-liquid flow pattern on initial bubble size". *Chinese Journal of Chemical Engineering*, **21(11)**, 1206–1215.

CHESTERS, A.K. (1991). "The modelling of coalescence processes in fluid-liquid dispersions: a review of current understanding". *Chemical engineering research and design*, **69(A4)**, 259–270.

COULALOGLOU, C.A. and TAVLARIDES, L.L. (1977). "Description of interaction processes in agitated liquid-liquid dispersions". *Chemical Engineering Science*, **32**, 1289–1297.

KATAOKA, I. and SERIZAWA, A. (1989). "Basic equations of turbulence in gas-liquid two-phase flow". *International Journal of Multiphase Flow*, **15**, 843–855.

LAAKKONEN, M., ALOPAEUS, V. and AITTAMAA, J. (2006). "Validation of bubble breakage, coalescence and mass transfer models for gas-liquid dispersion in agitated vessel". *Chemical Engineering Science*, **61**, 218–228.

LAAKKONEN, M., MOILANEN, P., ALOPAEUS, V. and AITTAMAA, J. (2007). "Modelling local bubble size distributions in agitated vessels". *Chemical Engineering Science*, **62**, 721–740.

LIAO, Y. and LUCAS, D. (2009). "A literature review of theoretical models for drop and bubble breakup in turbulent dispersions". *Chemical Engineering Science*, **64**, 3389–3406.

LIAO, Y. and LUCAS, D. (2010). "A literature review on mechanisms and models for the coalescence process of fluid particles". *Chemical Engineering Science*, **65**, 2851–2864.

LIAO, Y., RZEHAK, R., LUCAS, D. and KREPPER, E. (2015). "Baseline closure model for dispersed bubbly flow: Bubble coalescence and breakup". *Chemical Engineering Science*, **122**, 336–349.

LUCAS, D. and TOMIYAMA, A. (2011). "On the role of the lateral lift force in poly-dispersed bubbly flows". *International Journal of Multiphase Flow*, **37(9)**, 1178–1190.

LUCAS, D., KREPPER, E. and PRASSER, H.M. (2007). "Use of models for lift, wall and turbulent dispersion forces acting on bubbles for poly-disperse flows". *Chemical Engineering Science*, **62**, 4146–4157.

LUCAS, D., BEYER, M., SZALINSKI, P. and SCHUTZ, P. (2010). "A new database on the evolution of air-water flows along a large vertical pipe". *International journal of Thermal Sciences*, **49**, 664–674.

MARCHISIO, D.L. and FOX, R.O. (2013). *Computational Models for Polydisperse Particulate and Multiphase Systems*. Cambridge University Press, Cambridge, UK.

PRASSER, H.M., BEYER, M., BOTTGER, A., CARL, H., LUCAS, D., SCHAFFRATH, A., SCHUTZ, P., WEISS, F.P. and ZSCHAU, J. (2005). "Influence of the pipe diameter on the structure of the gas-liquid interface in a vertical two-phase pipe flow". *Nuclear Technology*, **152**, 3–22.

RAMKRISHNA, D. (2000). *Population balances: Theory and applications to particulate systems in engineering*. Academic press, San Diego, USA.

SCHAFFRATH, A., KRUSSENBERG, A., WEISS, F.P., HICKEN, E.F., BEYER, M., CARL, H., PRASSER, H., SCHUSTER, J., SCHUTZ, P., TAMME, M. *et al.* (2001). "Topflow-a new multipurpose thermalhydraulic test facility for the investigation of steady state and transient two phase flow phenomena". *Kerntechnik-Bilingual Edition-*, **66(4)**, 209–213.

SHAVER, D. and PODOWSKI, M. (2015). "Modeling and validation of forced convection subcooled boiling". *Proc. 16th Int. Topical Meeting on Nuclear Reactor Thermalhydraulics (NURETH-16), Chicago, IL.*

SUGRUE, R., MAGOLAN, B., LUBCHENKO, N. and BAGLIETTO, E. (2017). "Assessment of a simplified set of momentum closure relations for low volume fraction regimes in star-ccm+ and openfoam". *submitted to Annals of Nuclear Energy*.

TOMIYAMA, A., KATAOKA, I., ZUN, I. and SAKAGUCHI, T. (1998). "Drag coefficients of single bubbles under normal and micro gravity conditions". *JSME International Journal, Series B: Fluids and Thermal Engineering*, **41**, 472–479.

WANG, T., WANG, J. and JIN, Y. (2005). "Theoretical prediction of flow regime transition in bubble columns by the population balance model". *Chemical Engineering Science*, **60(22)**, 6199–6209.